AGU PUBLICATIONS

Geophysical Research Letters

RESEARCH LETTER

10.1002/2014GL061884

Key Points:
- Hot upwelling conduit was imaged beneath the Atlas Mountains
- High topography of the Atlas Mountains is due to active mantle support

Supporting Information:
- Readme
- Figure S1
- Figure S2
- Figure S3
- Figure S4
- Figure S5
- Figure S6
- Figure S7
- Figure S8
- Figure S9
- Figure S10

Correspondence to:
D. Sun,
daoyuans@usc.edu

Citation:
Sun, D., M. S. Miller, A. F. Holt, and T. W. Becker (2014), Hot upwelling conduit beneath the Atlas Mountains, Morocco, *Geophys. Res. Lett.*, *41*, 8037–8044, doi:10.1002/2014GL061884.

Received 16 SEP 2014
Accepted 24 OCT 2014
Accepted article online 29 OCT 2014
Published online 24 NOV 2014

Hot upwelling conduit beneath the Atlas Mountains, Morocco

Daoyuan Sun[1,2], Meghan S. Miller[1], Adam F. Holt[1], and Thorsten W. Becker[1]

[1]Department of Earth Sciences, University of Southern California, Los Angeles, California, USA, [2]Now at School of Earth and Space Sciences, University of Science and Technology of China, Hefei, China

Abstract The Atlas Mountains of Morocco display high topography, no deep crustal root, and regions of localized Cenozoic alkaline volcanism. Previous seismic imaging and geophysical studies have implied a hot mantle upwelling as the source of the volcanism and high elevation. However, the existence, shape, and physical properties of an associated mantle anomaly are debated. Here we use seismic waveform analysis from a broadband deployment and geodynamic modeling to define the physical properties and morphology of the anomaly. The imaged low-velocity structure extends to ~200 km beneath the Atlas and appears ~350 K hotter than the ambient mantle with possible partial melting. It includes a lateral conduit, which suggests that the Quaternary volcanism arises from the upper mantle. Moreover, the shape and temperature of the imaged anomaly indicate that the unusually high topography of the Atlas Mountains is due to active mantle support.

1. Introduction

The Atlas Mountains of Morocco are an intracontinental compressional belt formed by reactivation of Triassic-Jurassic age normal faults during the Cenozoic as Africa converged with Eurasia [*Brede et al.*, 1992; *Gomez et al.*, 2000; *Pique et al.*, 2002; *Teixell et al.*, 2003; *Arboleya et al.*, 2004]. It has high topography (up to 4100 m), yet displays relatively modest tectonic shortening (10–24%) [*Gomez et al.*, 1998; *Teixell et al.*, 2003] and no deep crustal root [*Sandvol et al.*, 1998; *Ayarza et al.*, 2005; *Zeyen et al.*, 2005; *Missenard et al.*, 2006; *Miller and Becker*, 2014]. Interpretation of structural seismology suggests that the lithosphere underneath the Atlas is thin, or the uppermost mantle abnormally hot, with low seismic velocities found at depths of ~65–160 km [*Seber et al.*, 1996; *Bijwaard and Spakman*, 2000; *Calvert et al.*, 2000; *Fullea et al.*, 2010; *Bezada et al.*, 2014]. Modeling indicates that the lithosphere is thinned (~65 km) compared with the thick lithosphere of the Saharan Platform and the Morocco Atlantic Margin along a corridor that is aligned with the highest topography in the Atlas [*Teixell et al.*, 2003, 2005; *Missenard et al.*, 2006; *Fullea et al.*, 2010; *Missenard and Cadoux*, 2012; *Miller and Becker*, 2014]. An anomalous lithosphere or mantle upwelling also explain the unusually high topography that is implied by the lack of a crustal root beneath the Atlas [*Teixell et al.*, 2005; *Missenard et al.*, 2006; *Frizon de Lamotte et al.*, 2009; *Fullea et al.*, 2010; *Miller and Becker*, 2014; *Zlotnik et al.*, 2014]. The source of the anomaly may be the Canary plume [*Anguita and Hernan*, 2000; *Duggen et al.*, 2009], associated with lithospheric delamination [*Duggen et al.*, 2009; *Bezada et al.*, 2014], or edge-driven convection [*Missenard and Cadoux*, 2012].

Geochemical analyses of the Quaternary basalts in the Middle Atlas also support the idea that the Canary Island plume is channeled beneath the Atlas. Recent alkali volcanism in the Middle Atlas has been suggested to be contemporaneous with recent uplift [*Anguita and Hernan*, 2000; *Duggen et al.*, 2009]. *S* receiver functions suggests that the lithosphere thickens sharply toward the north while crossing the northern margin of the Middle Atlas [*Miller and Becker*, 2014], i.e., from stations PM22 to PM21 in Figure 1a. Shear wave splitting analysis [*Miller et al.*, 2013] also indicates a strong change in azimuthal anisotropy strength at the northern edge of the Middle Atlas, as well as an alignment of fast polarization orientations parallel to the strike of topography, suggesting shearing in a mantle channel guided by lithospheric topography [*Alpert et al.*, 2013; *Miller et al.*, 2013; *Miller and Becker*, 2014].

Recent *P* wave [*Bezada et al.*, 2013, 2014] and surface wave [*Palomeras et al.*, 2014] tomography models have provided higher-resolution images of mantle structure beneath westernmost Mediterranean than previous work [e.g., *Seber et al.*, 1996; *Bijwaard and Spakman*, 2000; *Calvert et al.*, 2000] by using many temporary broadband stations. In the uppermost mantle beneath the Atlas, a low velocity anomaly (LVA) appears present in both tomography models. The *P* wave model indicates a LVA extending from a depth of 70 km to 200 km

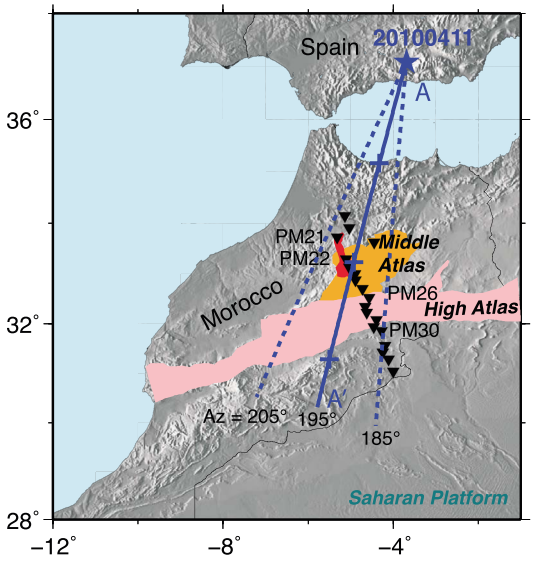

Figure 1. Map of seismic stations used in this study. Blue star denotes the deep Granada earthquake from 11 April 2010. Black inverted triangles indicate stations from the PICASSO seismic experiment. The pink patch outlines the High Atlas. Quaternary basalt outcrops are displayed as the red patch covering stations PM21 and PM22. Our study concentrated on the data between azimuth of 185° and 205°, which are modeled along the A-A′, 2-D profile.

beneath the Middle Atlas [*Bezada et al.*, 2014]. Surface wave tomography displays a much lower shear velocity at depths of 50 km to 150 km beneath the eastern Atlas [*Palomeras et al.*, 2014], in contrast to the western Atlas.

However, the inherently smooth images generated by traveltime tomography make it difficult to evaluate important details of the LVA, such as its spatial extent and velocity contrast. In contrast, the complementary information of waveform amplitudes and multipathing patterns provides such constraints and allows us to refine the tomographic models by waveform modeling. Here we present such an analysis and modeling of waveforms recorded in central and southern Morocco as applied to the LVA, providing further insight into the anomalous topography of the Atlas and the source of recent volcanism.

2. Regional and Teleseismic Earthquake Observations

We use the 2010 Granada earthquake (depth = 620 km, M_w = 6.2) [*Buforn et al.*, 2011; *Bezada and Humphreys*, 2012] recorded during PICASSO seismic deployment across the Atlas

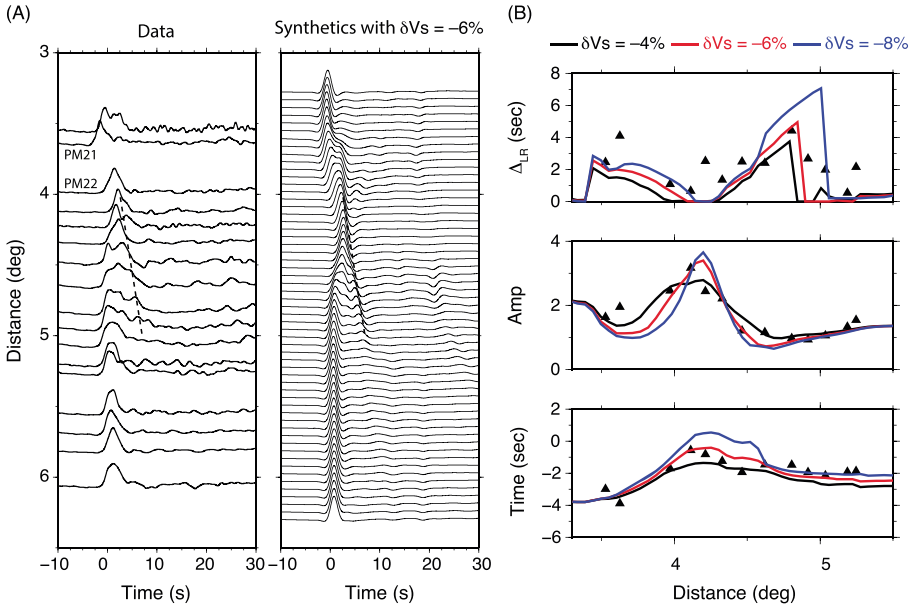

Figure 2. Comparison between *S* data (tangential component) and synthetics for the Granada earthquake. (a) The left column shows the data and the right column is the prediction from the preferred model in Figure 3a. The seismograms are aligned on the predicted arrival times from the AK135 model. The model predicts both the sharp change in the traveltime from stations PM21 to PM22 and the secondary arrivals (indicated by the dashed lines) at the distance range of 4.2–5°. (b) The differential time (Δ_{LR}) between the secondary arrival and the first arrival, amplitude, and traveltime of the data (black triangles) and the synthetics (lines). The black, red, and blue lines are predictions from the LVA with velocity perturbation of −4%, −6%, and −8%, respectively. To satisfy traveltimes and waveforms, a model with $\delta v_S = -6\%$ is preferred.

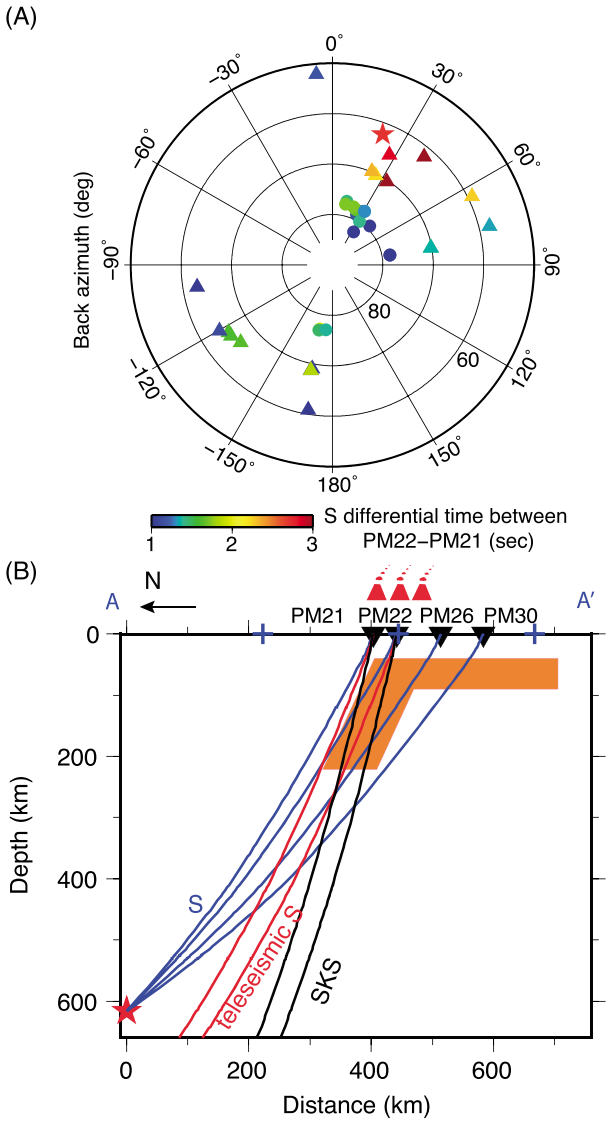

Figure 3. Teleseismic traveltimes and preferred model. (a) The *S* differential traveltime between stations PM22 and PM21 against the back azimuths of the events from station PM21. Both *S* (triangles) and *SKS* (circles) phases are used. The star represents the upgoing *S* phase of the deep Granada earthquake. The radius is the incident angle from horizontal at the depth of 120 km assuming the 1-D, AK135 reference model. The large time differences (red colors) are observed for events located at northeastern direction. Around back azimuth of 30°, several events have measurements for both *S* and *SKS*. (b) The preferred LVA model along the 2-D cross-section A-A′ in Figure 1a. Inside the orange box, the shear velocity perturbation is −6%. The Quaternary basalt outcrops (red volcano symbols) fall right above this low-velocity anomaly. The red star indicates the deep Granada earthquake, and the blue lines show the raypaths to the stations. The red and black lines show the raypaths for teleseismic *S* and *SKS*, respectively.

Mountains (Figure 1) as the only source event for waveform modeling. Such well-recorded deep earthquakes are rare, however, and each provides a unique opportunity to derive information about deep structure. In other words, any valid LVA model must explain the waveforms for this earthquake, which display three prominent features: First, from stations PM21 to PM22 at the northern margin of the Middle Atlas (Figure 1), *S* traveltime delays sharply increase to ~3 s (Figure 2a). Second, the southern stations at a distance range of 4.5 to 5° have a secondary late arrival, indicated by black dashed lines in Figure 2. Both waveform characteristics indicate a sharp boundary existing between stations PM21 and PM22, agreeing with the location of the LVA from tomography models. Third, the amplitude of the *S* arrivals peaks at 4° and decays with increasing distance (Figure 2).

Teleseismic events with good *P* and *S*/*SKS* arrivals are also used in our analysis (Figure 3). Because most traveltime variations occur between PM21 and PM22, we focus on the traveltime differences between those stations, and in particular the back azimuth-dependent delay times. The largest difference occurs for events coming from the northeast, although there are some variations. For the *SKS* phases (circles in Figure 3a; rays with incidence angles of ~80°), the traveltime differences are small and similar to those from other back azimuths (green and blue colors). In contrast, the time differences of *S*/*S*diff phases (triangles in Figure 3a) with shallower incidence angles display large anomalies of up to 3 s (red colors). For rays coming from the southwest, the differential times between stations are small, suggesting a northeast dipping anomaly.

3. Waveform Modeling

Because of the limited distribution of the stations, our structural model is simplified to two dimensions (2-D) along the profile A-A′ (Figure 1a). To generate synthetics, we applied a 2-D, staggered-grid finite difference scheme [*Li et al.*, 2014]. Figure S1 in the supporting information displays *SH* synthetics when using velocity anomalies from the *Bezada et al.* [2013] *P* tomography model, scaled by an approximate best fit value of 1.8. This structural model generally agrees with the observed traveltimes but is not able to explain the traveltime jump and secondary arrivals, which requires a model with sharper boundaries. To

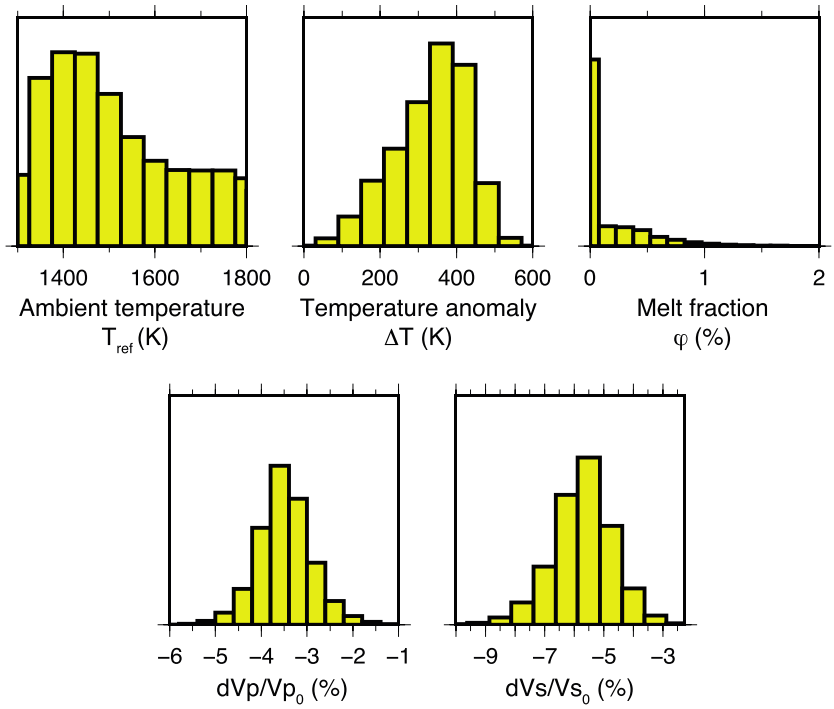

Figure 4. Histograms of estimates of T_{ref}, ΔT, φ, dVp/Vp_0, and dVs/Vs_0 from the Monte Carlo calculation. We chose the parameters at the depth of 140 km with the pressure of 4.5 GPa.

test such a model, we then assume that an LVA is the only anomaly below 40 km with uniform velocity perturbation from the AK135 model [*Kennett et al*., 1995] (Figure 3b). For the top 40 km, we use the surface tomography model based velocities [*Palomeras et al*., 2014].

The deep focus Granada earthquake has similar raypaths in the upper mantle to the teleseismic *S* phases with northeastern back azimuths (Figure 3b), and they display similar delay times (Figure 3a), suggesting a northeasterly dipping LVA (Figure 3b). Only if the rays are aligned along the sharp edge of the LVA can they produce significant traveltime differences as one ray will sample the slow anomaly and the other will sample the normal mantle [*Sun and Helmberger*, 2011] (Figure 3b). Furthermore, the greatly delayed *S*/*Sdiff* arrival times from stations PM21 to PM22 suggest that the dip angle of the LVA is 65° toward the northeast, which is similar to the previously mentioned teleseismic *S* raypaths. By matching the traveltimes, amplitudes, and the temporal separations between the second and first arrivals for all 15 stations along the profile (Figure 1) for the deep focus event, we find that a LVA centered beneath the High Atlas that is 200 km deep and 80 km wide, with shear wave velocity perturbation of −6% (Figure 3b), explains the observed waveforms well for both the local *S* and the delay times for teleseismic *S* and *SKS* (Figure 2). (Other models and resolution tests are discussed in Figures S2–S5 in the supporting information.)

The sharp northern boundary satisfies the ~3 s traveltime difference between stations PM21 and PM22 (Figure 2). Both stations PM21 and PM22 have simple waveforms, which indicate that the northern boundary of the LVA is located somewhere in between these stations. In the synthetics (spaced at 6 km), we do predict complicated waveforms at the distance range between stations PM21 and PM22. However, the distance between these two stations (~40 km) is too large to observe such features. In the model (Figure 3b), the sharp edges generate a diffracted wave and produce the observed secondary late arrivals (Figure 2a). Those secondary arrivals also support the inference that this anomaly is slow. Figure S6 presents an example of a conduit structure with the same dimension as the LVA in Figure 3b but shear wave velocity perturbation of +6%. Such a model fits the sharp traveltime change but fails to generate the strong secondary arrivals. Our preferred LVA model also explains the traveltimes of teleseismic *S* and *SKS*. Between stations PM21 to PM22, *SKS* traveltimes are essentially the same, yet the sharp *S* traveltime change causes *S-SKS* differential traveltime increase sharply (Figure S7).

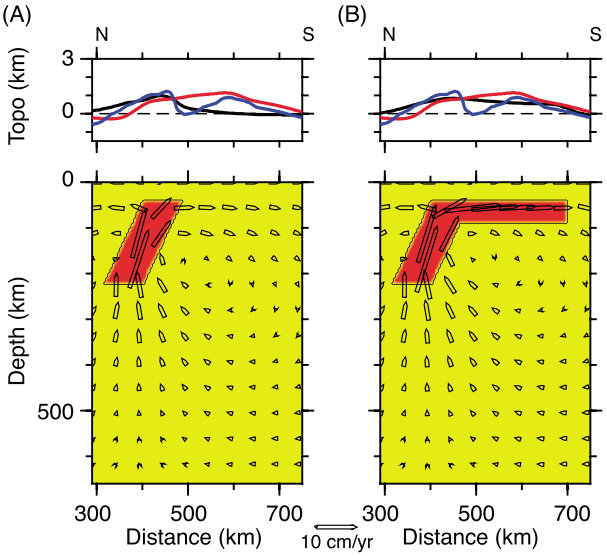

Figure 5. Predicted topography for the LVA model. (a) For a case where the LVA restricted to the Middle Atlas. (b) The LVA extends beneath the High Atlas (red patches in Figure 5b, bottom). Arrows indicate velocity vectors of associated mantle flow. In Figure 5b (top), the red line is real topography smoothed with 150 km wavelength filtering. For comparison with model predictions, the residual topography (blue line) is computed by correcting for Airy isostasy using *Ayarza et al.*'s [2014] Moho and assuming typical densities for crust (2800 kg/m^3) and mantle lithosphere (3250 kg/m^3). The black line is the predicted dynamic topography from the flow model.

Estimates for *P* and *S* velocities provide complementary constraints on the origin of the mantle anomalies [*Song and Helmberger*, 2007]. The differential *P* traveltimes for teleseismic events display less variations than for *S*, even for those events coming from the northeast (Figure S8). The *P* records of the Granada event do not have the second arrivals of the *S* data (Figure S9), which suggests that the *P* is much weaker than the *S* anomaly. We tested models with the same geometry as the *S* model and different *P* velocity perturbations. To match the amplitude variation across the profile, a model with *P* velocity drop of 3–4% is preferred (Figure S9).

4. Origin of the LVA

To explore the physical origin of the imaged velocity anomaly, we assume the anomaly has the same pyrolitic mantle composition as the ambient mantle and that the velocity of the LVA (V_{LVA}) is controlled by temperature variations (ΔT) and melt fraction (φ) with a correction from anelasticity [*Goes et al.*, 2000; *Karato and Karki*, 2001; *Cammarano et al.*, 2003], i.e., the velocity perturbation is given by

$$V_{\mathrm{LVA}} = \left(V_0 + \frac{\partial V}{\partial T}\Delta T + \frac{\partial V}{\partial \varphi}\varphi\right)\left(1 - \frac{Q^{-1}}{2\tan\left(\frac{\pi\alpha}{2}\right)}\right) \quad (1)$$

Here V_0 is the ambient *P* or *S* velocity for the AK135 model, α is a constant value of 0.15. Attenuation quality factor *Q* is a function of melting temperature T_m, seismic frequency, hydration, and temperature (ambient temperature T_{ref} plus ΔT) [*Goes et al.*, 2012]. The detailed parameters are listed in the supporting information. Because the effects of high water content on velocity are similar as those of partial melting [*Karato*, 2004], it is difficult to distinguish them from velocities alone. Thus, we assume a dry mantle.

To explore the plausible range of ΔT, T_{ref}, and φ that would explain the inferred LVA velocity anomalies, we performed 10^6 Monte Carlo simulations using equation (1) for *Vs* and V_P perturbations of −6% and −3.5%, respectively. In the simulations, if the temperature in the LVA is lower than T_m, then no partial melting appears ($\varphi = 0$). The results are displayed in Figure 4. The ambient temperature is poorly constrained with the most probable value of 1450 ± 150 K; bounds on the temperature anomaly are tighter with 350 ± 90 K. Most simulations suggest $\varphi = 0$ and the LVA may have a purely thermal origin. Thus, the temperature of the LVA would be ~1800 K, which is consistent with recent thermobarometry [*Thurner et al.*, 2014]. In Figure S10, we presented simulations for a hydrated mantle, which lower the melting temperature [*Hirth and Kohlstedt*, 1996] and *Q* value. The result shows similar ambient temperatures as dry mantle case but ΔT is 210 ± 80 K, consistent with modeling of hot spot tracks beneath the continental lithosphere [*Yang and Leng*, 2014]. The effects from volatile variations are difficult to evaluate. If the ambient mantle is hotter and dry, melt at the ~0.5% level may present (Figure 4). While there are uncertainties in estimating the effects from temperature and melt, we conclude that the LVA is likely due to a strong thermal anomaly and that partial melt may be present. A contribution of partial melt would also be consistent with results from magnetotellurics [*Anahnah et al.*, 2011].

5. Origin of Topography in the Atlas Mountains

To explore the dynamic implications of the LVA, we compute the mantle flow that would arise from the temperature anomaly and examine its surface expressions (Figure 5). We use the thermally induced density anomaly that corresponds to our best fit 350 K and compute an instantaneous, 2-D flow field, using the finite-element code CitcomCU [*Moresi and Solomatov*, 1995; *Zhong*, 2006]. For a background mantle viscosity of 5×10^{20} Pa s, we tested different viscosities of the LVA and found that this does not have a substantial large-scale effect but modulates details of the topographic expression, as expected.

Focusing on the nonflexurally supported, long-wavelength ($>$ ~150 km) topography, we compare the flow model predictions (dynamic topography) with actual, smoothed topography and with residual topography, i.e., actual topography minus the expected Airy isostatic signal using Moho depths from active source [*Ayarza et al*., 2014]. Dynamic topography is computed from the normal stresses at the free-slip upper surface of the model. Assuming a constant thermal expansion coefficient of 3×10^5 K^{-1}, the LVA anomaly corresponds to a density reduction of 40 kg/m^3, which fits the general amplitude of topography (~1.5 km, Figure 5a). When we confine the low-velocity structure to lie only beneath the Middle Atlas, the topography for the High Atlas is not matched well (Figure 5a). The predictions from our reference model (Figure 5b) match the topography across the whole Atlas Mountains. This suggests the presence of a low-velocity and positively buoyant mantle anomaly, which is not just a vertical conduit, but extends laterally to the High Atlas, and supports the high topography of the entire Atlas Mountains along this profile.

6. Discussion

Several mechanisms have been proposed to explain the evolution of the Atlas Mountains and the related thinned lithosphere, including edge-driven convection [e.g., *Fullea et al*., 2010; *Missenard and Cadoux*, 2012] and the rollback of the westernmost Mediterranean slab [*Frizon de Lamotte et al*., 2009] which may have facilitated lithospheric delamination and inflow of Canary plume [*Duggen et al*., 2009; *Bezada et al*., 2014], or a small plume from a deeper source [e.g., *Teixell et al*., 2005; *Zeyen et al*., 2005]. All models require different types of upwellings beneath the Atlas Mountains. First, an upwelling may indeed provide the dynamic support for the high topography across the Atlas. Second, a hot, active upwelling may alter the lithospheric strength, so enabling convective removal of the previously thickened lithosphere. The imaged LVA confirms such a hot upwelling beneath the Atlas Mountains. Receiver functions show the LVA connecting a deeper low velocity structure [*Miller et al*., 2014], which suggests the LVA is not an isolated anomaly. Intriguingly, we find that the Quaternary alkali volcanism is directly above the imaged, subvertical low-velocity anomaly (Figure 3b). This suggests that recent volcanism there may arise from the upper mantle at the depth of 200 km.

The conduit we image indicates a localized, hot upwelling, which seems incompatible with edge-driven convection [*Missenard and Cadoux*, 2012] where small-scale convection would form a broader and more diffuse low-velocity region. Instead, our results support the hypothesis that the High Atlas Mountains are supported by mantle inflow from the Canary hot spot [*Duggen et al*., 2009; *Miller and Becker*, 2014]. Such flow may cause, or be facilitated by, the delamination of mantle lithosphere beneath the High Atlas and so produce a corridor of thin lithosphere. Channeling of plume flow along this corridor then might have produced a series of small volcanic eruptions along zones of weakness in the lithosphere. Beneath the Middle Atlas, the subvertical upwelling flow provides a source for a large amount of mantle material undergoing decompression melting to generate the most voluminous Neogene volcanic field in northwestern Africa [*Duggen et al*., 2009, and references therein]. The velocity anomalies we image indicate that partial melting may still be occurring at depth. The low-velocity conduit is found to be tilted toward the north (Figure 3). This may imply that it is not only the Canary hot spot hot mantle source but also suction due to the rollback of the western Mediterranean that is shaping the Atlas Mountains [*Duggen et al*., 2009; *Alpert et al*., 2013; *Miller and Becker*, 2014].

7. Conclusions

Seismic waveforms recorded for the deep, 2010 Granada earthquake can be used to infer the nature of the mantle anomaly that underlies the Atlas Mountains. Detailed modeling of these waveforms allows us to constrain the physical properties of a low-velocity conduit which connects a zone at 200 km depth in the upper mantle to recent volcanism. Additional teleseismic *S* and *SKS* data further constrain the model

geometry and properties. This anomaly supports anomalously high topography of the Atlas Mountains and is a key piece of evidence further supporting a thinned lithosphere which is possibly related to plume-slab interactions.

Acknowledgments
The seismic data from the PICASSO array were accessed via the Data Management Center (DMC) of the Incorporated Research Institutions for Seismology (IRIS). This study was supported by the National Science Foundation, Continental Dynamics Program, under EAR-0809023. This study was also supported by USC postdoctoral scholar research grant. Comments by Editor Michael Wysession, Claire Currie, and one anonymous reviewer on an earlier version of the manuscript were motivating.

Michael Wysession thanks Claire A. Currie and one anonymous reviewer for their assistance in evaluating this paper.

References

Alpert, L. A., M. S. Miller, T. W. Becker, and A. A. Allam (2013), Structure beneath the Alboran from geodynamic flow models and seismic anisotropy, *J. Geophys. Res. Solid Earth*, *118*, 4265–4277, doi:10.1002/jgrb.50309.

Anahnah, F., et al. (2011), Deep resistivity cross section of the intraplate Atlas Mountains (NW Africa): New evidence of anomalous mantle and related Quaternary volcanism, *Tectonics*, *30*, TC5014, doi:10.1029/2010TC002859.

Anguita, F., and F. Hernan (2000), The Canary Islands origin: A unifying model, *J. Volcanol. Geoth. Res.*, *103*(1–4), 1–26.

Arboleya, M. L., A. Teixell, M. Charroud, and M. Julivert (2004), A structural transect through the High and Middle Atlas of Morocco, *J. Afr. Earth Sci.*, *39*(3-5), 319–327.

Ayarza, P., F. Alvarez-Lobato, A. Teixell, M. L. Arboleya, E. Teson, M. Julivert, and M. Charroud (2005), Crustal structure under the central High Atlas Mountains (Morocco) from geological and gravity data, *Tectonophysics*, *400*(1–4), 67–84.

Ayarza, P., et al. (2014), Crustal thickness and velocity structure across the Moroccan Atlas from long offset wide-angle reflection seismic data: The SIMA experiment, *Geochem. Geophys. Geosyst.*, *15*, 1698–1717, doi:10.1002/2013GC005164.

Bezada, M. J., and E. D. Humphreys (2012), Contrasting rupture processes during the April 11, 2010 deep-focus earthquake beneath Granada, Spain, *Earth Planet. Sci. Lett.*, *353*, 38–46.

Bezada, M. J., E. D. Humphreys, D. R. Toomey, M. Harnafi, J. M. Davila, and J. Gallart (2013), Evidence for slab rollback in westernmost Mediterranean from improved upper mantle imaging, *Earth Planet. Sci. Lett.*, *368*, 51–60.

Bezada, M. J., E. D. Humphreys, J. M. Davila, R. Carbonell, M. Harnafi, I. Palomeras, and A. Levander (2014), Piecewise delamination of Moroccan lithosphere from beneath the Atlas Mountains, *Geochem. Geophys. Geosyst.*, *15*, 975–985, doi:10.1002/2013GC005059.

Bijwaard, H., and W. Spakman (2000), Non-linear global P-wave tomography by iterated linearized inversion, *Geophys. J. Int.*, *141*(1), 71–82.

Brede, R., M. Hauptmann, and H. G. Herbig (1992), Plate tectonics and intracratonic mountain ranges in Morocco—The mesozoic-cenozoic development of the Central High Atlas and the Middle Atlas, *Geol. Rundsch.*, *81*(1), 127–141.

Buforn, E., C. Pro, S. Cesca, A. Udias, and C. del Fresno (2011), The 2010 Granada, Spain, deep earthquake, *Bull. Seismol. Soc. Am.*, *101*(5), 2418–2430.

Calvert, A., E. Sandvol, D. Seber, M. Barazangi, F. Vidal, G. Alguacil, and N. Jabour (2000), Propagation of regional seismic phases (Lg and Sn) and Pn velocity structure along the Africa-Iberia plate boundary zone: Tectonic implications, *Geophys. J. Int.*, *142*(2), 384–408.

Cammarano, F. S., P. V. Goes, and D. Giardini (2003), Inferring upper-mantle temperatures from seismic velocities, *Phys. Earth Planet. Inter.*, *138*, 197–222.

Duggen, S., K. A. Hoernle, F. Hauff, A. Klugel, M. Bouabdellah, and M. F. Thirlwall (2009), Flow of Canary mantle plume material through a subcontinental lithospheric corridor beneath Africa to the Mediterranean, *Geology*, *37*(3), 283–286.

Frizon de Lamotte, D., P. Leturmy, Y. Missenard, S. Khomsi, G. Ruiz, O. Saddiqi, F. Guillocheau, and A. Michard (2009), Mesozoic and Cenozoic vertical movements in the Atlas system (Algeria, Morocco, Tunisia): An overview, *Tectonophysics*, *475*(1), 9–28.

Fullea, J., M. Fernandez, J. C. Afonso, J. Verges, and H. Zeyen (2010), The structure and evolution of the lithosphere-asthenosphere boundary beneath the Atlantic-Mediterranean Transition Region, *Lithos*, *120*(1-2), 74–95.

Goes, S., R. Govers, and P. Vacher (2000), Shallow mantle temperatures under Europe from P and S wave tomography, *J. Geophys. Res.*, *105*(B5), 11,153–11,169, doi:10.1029/1999JB900300.

Goes, S., J. Armitage, N. Harmon, H. Smith, and R. Huismans (2012), Low seismic velocities below mid-oceanic ridges: Attenuation versus melt retention, *J. Geophys. Res.*, *117*, B124013, doi:10.1029/2012JB009637.

Gomez, F., R. Allmendinger, M. Barazangi, A. Er-Raji, and M. Dahmani (1998), Crustal shortening and vertical strain partitioning in the Middle Atlas Mountains of Morocco, *Tectonics*, *17*(4), 520–533, doi:10.1029/98TC01439.

Gomez, F., W. Beauchamp, and M. Barazangi (2000), Role of the Atlas Mountains (northwest Africa) within the African-Eurasian plate-boundary zone, *Geology*, *28*(9), 775–778.

Hirth, G., and D. L. Kohlstedt (1996), Water in the oceanic upper mantle: Implications for rheology, melt extraction and the evolution of the lithosphere, *Earth Planet. Sci. Lett.*, *144*, 93–108.

Karato, S. and B. B. Karki (2001), Origin of lateral variation of seismic wave velocities and density in the deep mantle, *J. Geophys. Res.*, *106*(B10), 21,771–21,783, doi:10.1029/2001JB000214.

Karato, S.-I. (2004), Mapping water content in the upper mantle, in *Inside the Subduction Factory*, edited by J. Eiler, AGU, Washington, D. C., doi:10.1029/138GM08.

Kennett, B. L. N., E. R. Engdahl, and R. Buland (1995), Constraints on seismic velocities in the Earth from travel times, *Geophys. J. Int.*, *122*, 108–124.

Li, D., D. Helmberger, R. W. Clayton, and D. Sun (2014), Global synthetic seismograms using a 2-D finite-difference method, *Geophys. J. Int.*, *197*(2), 1166–1183, doi:10.1093/gji/ggu1050.

Miller, M. S., and T. W. Becker (2014), Reactivated lithospheric-scale discontinuities localize dynamic uplift of the Moroccan Atlas Mountains, *Geology*, *42*(1), 35–38.

Miller, M. S., A. A. Allam, T. W. Becker, J. F. Di Leo, and J. Wookey (2013), Constraints on the tectonic evolution of the westernmost Mediterranean and northwestern Africa from shear wave splitting analysis, *Earth Planet. Sci. Lett.*, *375*, 234–243.

Miller, M. S., D. Sun, L. J. O'Driscoll, T. W. Becker, A. Holt, A. J. Butcher, J. Diaz, and C. Thomas (2014), Imaging the upper mantle low velocity zones and conduits beneath the Atlas Mountains of Morocco: Links to volcanism and orogenesis, *Geol. Soc. Am. Abstracts with Programs*, 46(6), 403, Paper No. 159–9.

Missenard, Y., and A. Cadoux (2012), Can Moroccan Atlas lithospheric thinning and volcanism be induced by edge-driven convection?, *Terra Nova*, *24*(1), 27–33.

Missenard, Y., H. Zeyen, D. F. de Lamotte, P. Leturmy, C. Petit, M. Sebrier, and O. Saddiqi (2006), Crustal versus asthenospheric origin of relief of the Atlas Mountains of Morocco, *J. Geophys. Res.*, *111*, B03401, doi:10.1029/2005JB003708.

Moresi, L.-N., and V. S. Solomatov (1995), Numerical investigation of 2D convection with extremely large viscosity variations, *Phys. Fluids*, *7*, 2154–2162.

Palomeras, I., S. Thurner, A. Levander, K. Liu, A. Villasenor, R. Carbonell, and M. Harnafi (2014), Finite-frequency Rayleigh wave tomography of the western Mediterranean: Mapping its lithospheric structure, *Geochem. Geophys. Geosyst.*, *15*, 140–160, doi:10.1002/2013GC004861.

Pique, A., P. Tricart, R. Guiraud, E. Laville, S. Bouaziz, M. Amrhar, and R. A. Ouali (2002), The Mesozoic-Cenozoic Atlas belt (North Africa): An overview, *Geodin. Acta*, *15*(3), 185–208.

Sandvol, E., D. Seber, A. Calvert, and M. Barazangi (1998), Grid search modeling of receiver functions: Implications for crustal structure in the Middle East and North Africa, *J. Geophys. Res.*, *103*(B11), 26,899–26,917, doi:10.1029/98JB02238.

Seber, D., M. Barazangi, B. A. Tadili, M. Ramdani, A. Ibenbrahim, and D. Ben Sari (1996), Three-dimensional upper mantle structure beneath the intraplate Atlas and interplate Rif mountains of Morocco, *J. Geophys. Res.*, *101*(B2), 3125–3138, doi:10.1029/95JB03112.

Song, T. R. A., and D. V. Helmberger (2007), A depleted, destabilized continental lithosphere near the Rio Grande rift, *Earth Planet. Sci. Lett.*, *262*(1-2), 175–184.

Sun, D., and D. Helmberger (2011), Upper-mantle structures beneath USArray derived from waveform complexity, *Geophys. J. Int.*, *184*(1), 416–438.

Teixell, A., M. L. Arboleya, M. Julivert, and M. Charroud (2003), Tectonic shortening and topography in the central High Atlas (Morocco), *Tectonics*, *22*(5), 1051, doi:10.1029/2002TC001460.

Teixell, A., P. Ayarza, H. Zeyen, M. Fernandez, and M. L. Arboleya (2005), Effects of mantle upwelling in a compressional setting: The Atlas Mountains of Morocco, *Terra Nova*, *17*(5), 456–461.

Thurner, S., I. Palomeras, A. Levander, R. Carbonell, and C.-T. Lee (2014), Ongoing lithospheric removal in the western Mediterranean: Evidence from Ps receiver functions and thermobarometry of Neogene basalts (PICASSO project), *Geochem. Geophys. Geosyst.*, *15*, 1113–1127, doi:10.1002/2013GC005124.

Yang, T., and W. Leng (2014), Dynamics of hidden hotspot tracks beneath the continental lithosphere, *Earth Planet. Sci. Lett.*, *401*, 294–300.

Zeyen, H., P. Ayarza, M. Fernandez, and A. Rimi (2005), Lithospheric structure under the western African-European plate boundary: A transect across the Atlas Mountains and the Gulf of Cadiz, *Tectonics*, *24*, TC2001, doi:10.1029/2004TC001639.

Zhong, S. J. (2006), Constraints on thermochemical convection of the mantle from plume heat flux, plume excess temperature, and upper mantle temperature, *J. Geophys. Res.*, *111*, B04409, doi:10.1029/2005JB003972.

Zlotnik, S., I. Jimenez-Munt, and M. Fernandez (2014), Coupled mantle dripping and lateral dragging controlling the lithosphere structure of the NW-Moroccan margin and the Atlas Mountains: A numerical experiment, *Lithos*, *189*, 16–27.